ACS Photonics

Open Access

pubs.acs.org/journal/apchd5

Article

From Free Space to Guided Modes: Tunable and Directional Coupling with Microsphere Resonators

Rohit B. Raj, Jaime Rivera, Esther Alarcón-Lladó, Sachin Kinge, and Erik C. Garnett*

Cite This: *ACS Photonics* 2026, 13, 4966−4973

Read Online

ACCESS | Metrics & More | Article Recommendations | Supporting Information

ABSTRACT: Efficiently interfacing free-space light with subwavelength waveguides remains a major challenge in integrated photonics, particularly at visible wavelengths relevant for spectroscopy and photocatalysis. We demonstrate a lithography-free coupling strategy using individual silica (SiO_2) microspheres integrated onto suspended silicon nitride (Si_3N_4) membranes. When illuminated with a focused Gaussian beam, the microspheres excite resonances that evanescently couple into the underlying waveguide with efficiencies up to 50%, as measured by integrating-sphere microscopy. The coupled spectrum spans 500−780 nm, and axial beam translation reproducibly shifts the dominant wavelength from 550 to 710 nm, providing straightforward spectral tunability. Crucially, both experiments and full-field simulations reveal that the in-coupled light is launched directionally, while the wavelength-matched out-coupling and in-coupling efficiencies show excellent agreement, consistent with reciprocity. This combination of broadband operation, postfabrication tunability, and controlled directionality establishes microsphere coupling as a reconfigurable route for visible-light integrated photonics, enabling selective light delivery for chip-based photocatalysis and multiplexed lab-on-chip spectroscopy.

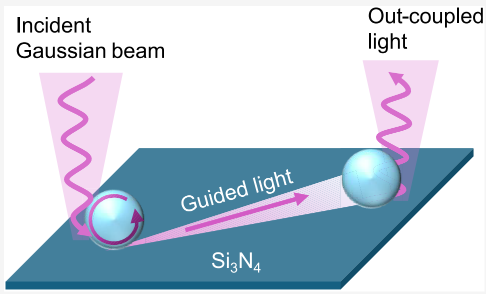

KEYWORDS: *whispering-gallery mode, in-coupling efficiency, directionality, silicon nitride, microspheres, evanescent coupling*

■ INTRODUCTION

Integrated photonics promises compact, high-bandwidth platforms for communications and spectroscopy, yet remains constrained by the difficulty of coupling free-space or fiber light into submicron waveguides.[1−3] While these waveguides enable low-loss, densely integrated devices, their mode profiles are severely mismatched to ∼10 μm free-space or fiber modes, yielding only ∼1% coupling without dedicated structures.[4−7] To overcome this mismatch, lithographic edge couplers, such as inverse tapers, expand the on-chip mode, routinely achieving efficiencies greater than 90% with broad bandwidths.[8,9] Grating couplers, which diffract normally incident light into the waveguide plane, simplify wafer-scale testing but typically deliver efficiencies of around 60−70% in Si_3N_4 with bandwidths of 40−100 nm.[10] While these devices are highly effective for fixed band datacom, all lithographic couplers are inherently static: once fabricated, their wavelength acceptance and output direction cannot be adjusted.[3,10,11] This immutability limits applications requiring postfabrication wavelength selectivity or directional routing.

One emerging area that highlights this limitation is chip-based photocatalysis.[10,12−14] Photocatalytic reactions rely on nanostructures with sharp-wavelength-dependent absorption. Plasmonic Au and Ag nanoparticles exhibit resonance across the visible to near-infrared (NIR) region, depending on their geometry and environment,[15,16] whereas semiconductor catalysts, such as TiO_2, require ultraviolet excitation.[17,18] Delivering light selectively at these resonances and routing it to distinct regions on-chip would enable programmable or multiplexed reactivity.[19−21] A similar need arises in lab-on-chip spectroscopy,[22−25] where distinct analytes or detector elements benefit from site-specific illumination.

Microspheres provide an alternative route toward reconfigurable coupling. Braginsky et al. first established dielectric microspheres as ultrahigh-Q resonators,[26] while Cai et al. later demonstrated near-unity coupling efficiency with tapered fibers,[27] laying the foundation for their use as versatile coupling elements. Building on this foundation, Shu et al. experimentally achieved 16.8% (per direction) by coupling a focused free-space laser into a silica microsphere and collecting through a single-mode fiber at 1550 nm.[28] Beyond fiber geometries, attention has shifted to planar waveguides. Tsintzos et al. simulated the coupling of quantum-dot emission from nanowires into silica-on-silicon waveguides via a microsphere, predicting coupling efficiencies of ∼40−50% across the 880−940 nm range.[29] Kushwaha et al. reported nanojet-mediated in-coupling into glass slab waveguides in the

Received: November 20, 2025
Revised: June 23, 2026
Accepted: June 24, 2026
Published: August 13, 2026

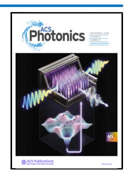

https://doi.org/10.1021/acsphotonics.5c02800
ACS Photonics 2026, 13, 4966−4973

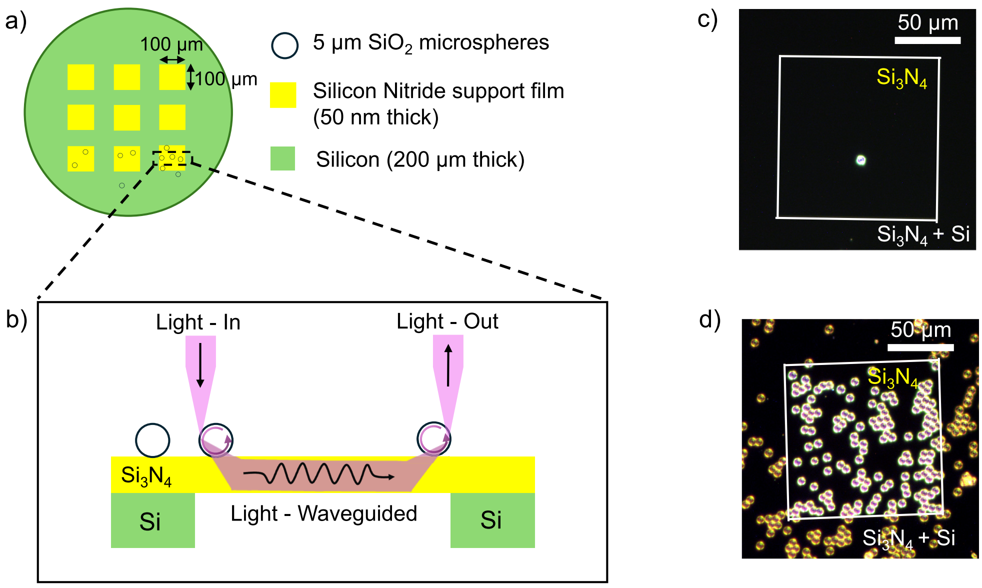

Figure 1. Tunable in-coupler design: (a) Schematic of 5 μm SiO_2 microspheres stamped on a TEM grid used to study both in and out-coupling of light. (b) Light is coupled into the Si_3N_4 waveguide by one microsphere, followed by distal out-coupling at another microsphere or absorption when it reaches the Si support. Dark-field optical images: (c) isolated 5 μm SiO_2 microsphere on a Si_3N_4 membrane; (d) uniform distribution of microspheres on the suspended Si_3N_4 membrane (waveguide) and on the Si_3N_4 thin film on Si substrate. The dashed white line shows the border of one suspended membrane.

800−880 nm range.[30] Most importantly, Ogura et al. studied polystyrene microspheres on ultrathin Si_3N_4 films and reported qualitative control of guided-light directionality under 532 nm excitation.[31] Collectively, these works demonstrate the versatility of microspheres. However, in planar waveguide platforms operating at visible wavelengths, the evidence remains qualitative or simulated, with no quantitative demonstration of absolute efficiencies, broadband wavelength tunability, or controlled directional launching.

Here, we establish a lithography-free microsphere−waveguide platform that directly addresses these gaps. By integrating SiO_2 microspheres onto suspended 50 nm Si_3N_4 membranes and interrogating them with a custom integrating-sphere microscope, we quantify free-space coupling efficiency, spectral tunability, and directionality in these nanophotonic waveguides. Focused Gaussian illumination excites overlapping morphology-dependent Mie resonances, with the efficiently guided-coupled resonances identified as whispering gallery mode (WGM)-like resonances that evanescently transfer energy into guided modes spanning 500−780 nm. Translating the incident beam continuously tunes the dominant coupled wavelength from 550 to 710 nm, while positioning the focused beam at different azimuthal locations around the microsphere rim enables unidirectional launching in any preferred direction within the membrane plane. Absolute in-coupling efficiencies approach 50%, which, to the best of our knowledge, is among the highest values reported for free-space coupling into Si_3N_4 waveguides in the visible range (500−780 nm). Full-field simulations support this result by identifying the WGM-mediated coupling pathway and confirming directional launching into the waveguide. Crucially, this performance approaches that of advanced Si_3N_4 grating couplers in the visible range (59% efficiency with a bandwidth of approximately 50 nm),[32] yet it is achieved without lithography and with postfabrication reconfigurability.

These results establish microsphere coupling as a versatile strategy for visible-light integrated photonics. By uniting high efficiency with broadband tunability and directional control, our approach opens pathways toward reconfigurable on-chip platforms for photocatalysis, multiplexed spectroscopy, and other applications that require selective light delivery beyond the static limits of lithographically fabricated couplers.

■ RESULTS AND DISCUSSION

The substrate consists of a 50 nm-thick Si_3N_4 thin film, which serves as the optical waveguide due to its low optical losses and mechanical robustness.[33,34] This film is deposited on a 200 μm thick Si wafer that has nine 100 μm × 100 μm etched windows, leaving suspended Si_3N_4 membranes in those regions (Figure 1a). SiO_2 microspheres with a diameter of 5 μm deposited onto the substrate act as free-space light in-couplers (see Section 1 of the Supporting Information (SI) for fabrication details). The microsphere efficiently couples the Gaussian beam into the waveguide through morphology-dependent Mie resonances. In dielectric microspheres, WGMs correspond to the high-angular-order subset of these resonances, with fields localized near the sphere periphery.[35−37] In our excitation geometry, these WGMs trap and guide the incoming beam along the microsphere's circumference, with a fraction of the trapped light leaking into the waveguide via evanescent-field coupling.

Figure 1b provides a schematic illustration of the experimental configuration used to monitor the propagation direction of the in-coupled light and quantify the in-coupling and out-coupling efficiency. Light coupled in at the edge of one silica microsphere propagates through the waveguide until it reaches another silica microsphere, where it is out-coupled to the far field or the silicon substrate, where it is absorbed. A single 5 μm SiO_2 microsphere placed onto the waveguide is used to quantify the efficiency of light in-coupling by assuming that all waveguided light is absorbed by the silicon substrate when it reaches the end of the suspended membrane (Figure 1c). In contrast, multiple microspheres uniformly placed on the waveguide act as discrete out-couplers of light, which are

https://doi.org/10.1021/acsphotonics.5c02800
ACS Photonics 2026, 13, 4966−4973

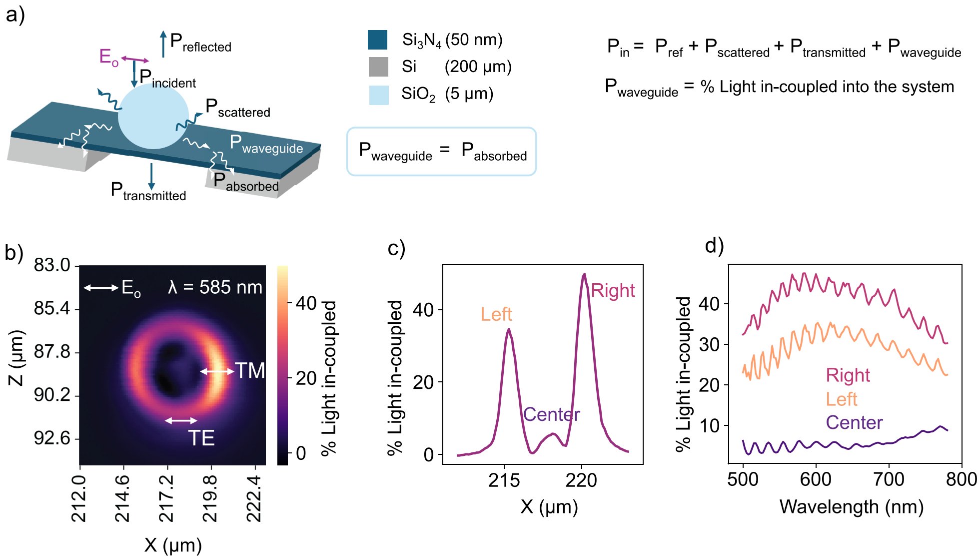

Figure 2. Light in-coupled into the waveguide by a 5 μm SiO_2 microsphere. (a) Schematic illustrating different pathways of light interaction with the system. (b) Spatial profile of the in-coupled light at different locations on the microsphere when illuminated at the 585 nm resonance wavelength. (c) Line profile of in-coupled light along the microsphere's center. (d) Wavelength-dependent in-coupling efficiency at the left edge, right edge, and center of the microsphere.

used to image the directionality of the in-coupled and guided light (Figure 1d). Finally, as an initial step toward plasmon-mediated catalysis using guided modes, we demonstrate the excitation of gold nanocubes (AuNCs). For these experiments, AuNCs were first deposited onto the waveguide surface by drop-casting, after which multiple SiO_2 microspheres were transferred onto the surface, with one microsphere acting as the primary light in-coupler.

Light In-Coupling Experiments

A custom-built integrating-sphere microscope is used to quantify light in-coupling efficiency by placing a single SiO_2 microsphere on a 50 nm-thick suspended Si_3N_4 membrane (see Section 2 in SI for details of the experimental setup and calculations). When the microsphere is illuminated with a focused beam of power P_{in}, part of the light is scattered into the air ($P_{scattered}$), and part of it is scattered into the waveguide at a sufficiently large angle that it becomes trapped ($P_{waveguide}$). The in-coupled light propagates through the waveguide and is eventually absorbed by the Si substrate, due to its large absorption coefficient (~10^4−10^3 cm^{-1} at 500−780 nm).[38] The remaining light does not interact with the microsphere and is either reflected ($P_{reflected}$) or transmitted ($P_{transmitted}$) through the substrate. Therefore, the fraction of light in-coupled into the waveguide can be calculated by

$$\frac{P_{waveguide}}{P_{in}} = 1 - \frac{P_{scattered}}{P_{in}} - \frac{P_{reflected}}{P_{in}} - \frac{P_{transmitted}}{P_{in}} \tag{1}$$

Efficient light in-coupling into the waveguide requires optimal excitation of the microsphere's peripheral, high-angular-order WGMs. The WGMs are most efficiently excited when the incident Gaussian beam is focused at the sphere's equatorial periphery.[35−37] To concentrate the light at the equator of the microsphere, which has a diameter of ~5 μm, we focus the Gaussian beam roughly 2.5 μm above the waveguide. At this height, the beam overlaps maximally with the sphere's edge, driving the high-Q circulating WGMs (Q is defined as E_{res}/FWHM, where E_{res} is the resonance energy of the WGM and FWHM is the full-width at half-maximum). In simulations, these modes exhibited Q values ranging from 364 to 1924 (SI, Figure S5). The trapped light could then extend an evanescent field tens of nanometers beyond the sphere's surface, where it overlaps with and couples to a mode in the adjacent Si_3N_4 waveguide, achieving efficient energy transfer.[39]

The microsphere was excited with linearly polarized light at $\lambda \sim 585$ nm, with the electric field aligned parallel to the waveguide as illustrated in Figure 2a,b. Following the standard WGM convention, transverse electric (TE) WGMs are defined as those with electric fields tangential to the sphere surface ($E_r = 0$, where E_r denotes the radial electric-field component), while transverse magnetic (TM) WGMs possess a radial electric field component ($E_r \neq 0$).[40,41] Figure 2b presents the spatial profile of in-coupled light at the microsphere's equatorial plane, obtained by raster-scanning the focal spot in steps of 100 nm. The maximum in-coupling efficiency of 50% is measured at the edges of the sphere. This is further illustrated in Figure 2c, where a line cut through the microsphere center reveals two distinct peaks, corresponding to in-coupling at the left and right edges. At the left and right edges, the incident polarization projects radially with respect to the local sphere surface, thereby exciting TM modes, which couple efficiently into the waveguide.[42,43] In contrast, at the top and bottom edges, the polarization projects tangentially, corresponding to TE modes, which exhibit weaker coupling.[42,43] Excitation at the center of the microsphere resulted in a substantial decrease in in-coupling efficiency to approximately 6%, highlighting the spatial sensitivity of the coupling mechanism and supporting preferential excitation of peripheral WGM resonances when the beam overlaps with the microsphere rim. A comparable maximum in-coupling efficiency was obtained from an additional microsphere from the same batch, reaching 48%, close to the 50% maximum measured for the representative sphere (SI, Figure S10).

Figure 2d plots the wavelength-dependent in-coupling efficiency at different positions on the microsphere. When the excitation beam is focused near the sphere's edge, the

https://doi.org/10.1021/acsphotonics.5c02800
ACS Photonics 2026, 13, 4966−4973

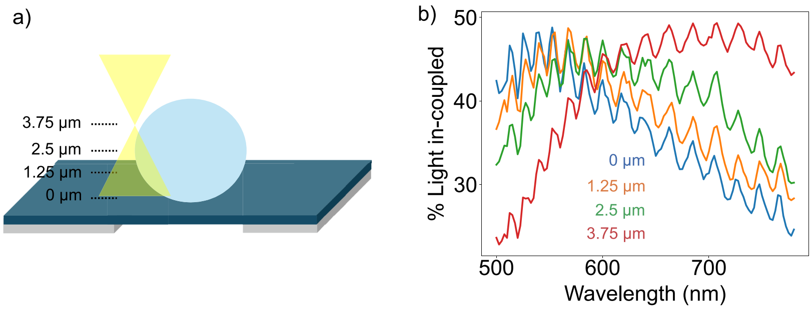

Figure 3. Tuning the peak in-coupled wavelength via axial focus. (a) Schematic of the Gaussian-beam waist positions relative to the Si_3N_4 membrane. The axial coordinate z_0 is defined normal to the Si_3N_4 membrane plane. The beam waist positions are z_0 = 0, 1.25, 2.5, and 3.75 μm, with z_0 = 2.5 μm corresponding approximately to the microsphere equator. (b) Corresponding waveguide in-coupling spectra showing a monotonic shift of the spectral maximum with focus height.

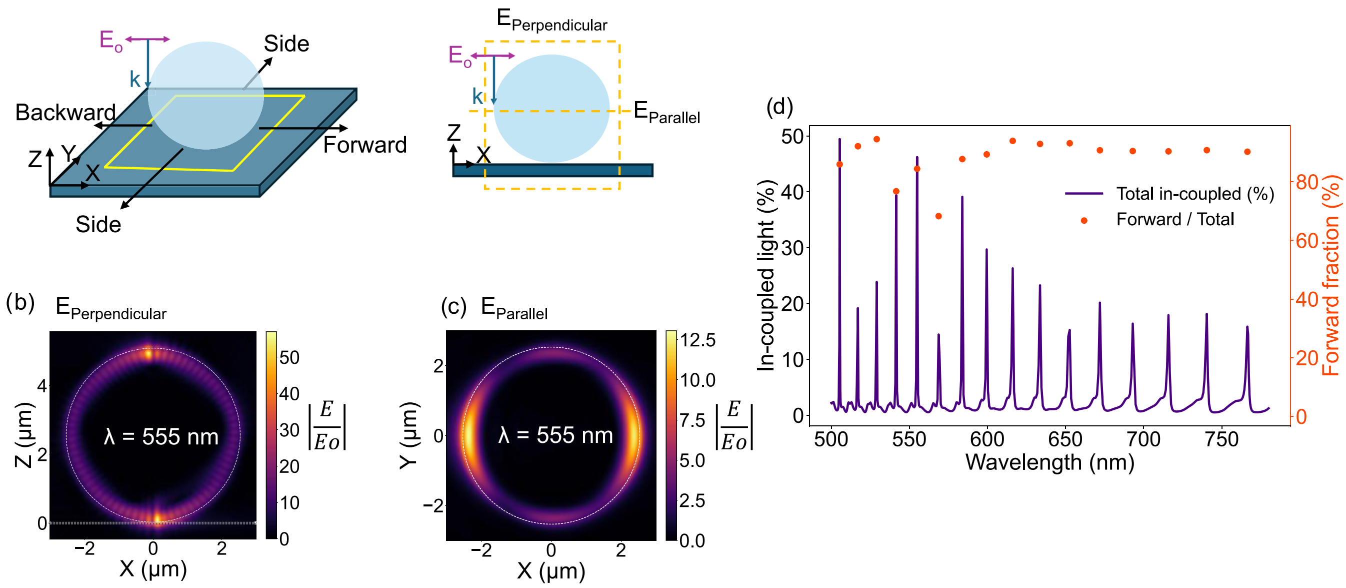

Figure 4. Simulation of light in-coupling into the waveguide by a single SiO_2 microsphere. (a) Schematic of the excitation setup: frequency-domain field and power monitors are positioned within the waveguide to measure the fraction of light coupled into it. (b) 2D Electric field distribution at the sphere−waveguide interface: visualization of light interaction at the coupling region. (c) Cross-sectional field profile of the microsphere: representation of how light is distributed inside and around the sphere. White outlines indicate the sphere and waveguide. (d) Wavelength-dependent in-coupling efficiency, with total in-coupled light (purple, left axis) and forward fraction (orange, scatter, right axis).

spectrum exhibits a series of narrow, periodic resonances superimposed on a broad envelope, with the overall coupling maximum centered at λ_{max} = 585 nm. These sharp periodic resonances, together with the edge-selective excitation response, are characteristic of WGMs, which originate from constructive interference of light confined within the sphere by total internal reflection.[44] We analyze the fine spectral structure by fitting each resonance with a Lorentzian line shape, thereby determining its resonance wavelength (λ_{res}), FWHM, and corresponding Q-factors. The average spacing between adjacent WGMs is approximately 57 meV. The complete set of the extracted spectral parameters is provided in Table S1 of the SI.

The broad underlying envelope arises from the interplay of two coupling processes: (i) free-space excitation of multiple WGMs in the microsphere and (ii) evanescent transfer from those WGMs into the waveguide mode of the 50 nm Si_3N_4 membrane.[45−48] Within this interplay, the WGM whose tangential propagation constant and near-field overlap best match the guided mode couples most strongly, producing a dominant maximum at λ_{max}. Neighboring modes contribute progressively less, shaping the overall spectral envelope.[47,49] Sixteen resonances are resolved in the measured spectrum (Figure 2d, left), and full-field simulations at 555, 600, and 715 nm (SI, Figure S6) confirm distinct surface-field distributions with varying field profiles at the microsphere−waveguide interface.

We systematically shifted the axial focus from 0 to 3.75 μm by varying the position of the Gaussian beam waist relative to the Si_3N_4 membrane (Figure 3a). This tuning reproducibly reweighed the coupling channels and shifted the spectral envelope maximum from 550 to 710 nm (Figure 3b). This shift occurs because tuning the focus alters the tangential wavevector distribution at the microsphere−waveguide interface,[36,50,51] thereby changing the relative efficiencies with which neighboring WGMs couple into the guided mode. Such behavior is consistent with prior free-space studies, where modest changes in excitation position,[30,52] impact parameter (beam-to-rim offset),[36] or injection angle[53] selectively enhanced or suppressed different WGM families, altering observed line shapes from Lorentzian to Fano-like[52] without shifting the eigenfrequencies themselves. It is further supported

https://doi.org/10.1021/acsphotonics.5c02800
ACS Photonics 2026, 13, 4966−4973

by position-dependent coupling studies in microsphere−waveguide systems, where varying the sphere−waveguide gap and the transverse offset of the microsphere relative to the waveguide core systematically reweights closely spaced WGMs, modifying their relative coupling efficiencies while the resonance positions remained fixed.[49] On our platform, axial focus thus provides a single, robust control that redistributes power among accessible WGMs and deterministically enhances those that couple most efficiently into the waveguide.

Simulation of Light In-Coupling by a Single Microsphere

We employed three-dimensional finite-difference time-domain (3D FDTD) simulations using Lumerical to model light in-coupling into the waveguide mediated by a single microsphere. A 5.067 μm diameter SiO_2 sphere was placed on a 50 nm-thick Si_3N_4 membrane and illuminated with a linearly polarized Gaussian beam focused at the sphere's equator (Figure 4a). Motivated by the experimental observation that radial field projection at the left and right edges produces stronger coupling than tangential projection at the top and bottom edges, the simulated incident electric field was oriented radially with respect to the local microsphere surface. This configuration selectively probes the TM-like coupling pathway that is most efficient for evanescent transfer into the underlying Si_3N_4 waveguide.[44,45] The simulated sphere diameter was chosen to match the experimentally measured value from a scanning electron microscope (SEM) image (SI, Figure S1d).

To analyze the modal field structure of the resonances, we position two electric-field monitors in the simulation: one oriented parallel to the waveguide plane at the microsphere's equator, E_{parallel}, and the other perpendicular to the waveguide plane passing through the sphere's center, $E_{\text{perpendicular}}$. For a resonant wavelength of 555 nm, the $E_{\text{perpendicular}}$ monitor revealed periodic electric-field maxima and minima around the sphere's circumference (Figure 4b), consistent with high-angular-order circulating modes. Complementarily, the E_{parallel} monitor showed strong field enhancement localized at the sphere's rim (Figure 4c). Together, the circumferential field periodicity and rim-localized enhancement identify the efficiently coupled simulated resonances as WGMs. Notably, in the $E_{\text{perpendicular}}$ monitor, the strongest enhancements were observed at both the upper and lower edges of the microsphere, with the lower edge field penetrating the underlying waveguide. This spatial asymmetry arises due to the broken radial symmetry induced by the presence of the underlying high-index Si_3N_4 membrane.[54] Such symmetry breaking is advantageous, as it facilitates efficient evanescent-field coupling and optimal phase matching between the WGMs and the guided modes of the waveguide, significantly enhancing the microsphere's overall light-in-coupling efficiency.[50]

The spectral characteristics of the in-coupling were then evaluated. Figure 4d (solid line, purple) presents the simulated wavelength-dependent light in-coupling efficiency over the 500−780 nm spectral range. The spectrum consists of a series of discrete, sharply defined resonances with periodic spacing, forming an overall peak envelope that qualitatively follows the experimental response in Figure 2d. Each resonance was fitted with a Lorentzian line shape to extract the resonance wavelength λ_{res}, FWHM, and Q. A complete set of these spectral parameters is provided in Table S2 of the SI.

Although the simulated and experimental spectra show a similar overall spectral shape, the experimental resonances are noticeably broader and partially overlap with each other. We suggest that this spectral broadening can be attributed primarily to two factors: (i) the finite spectral bandwidth of the excitation laser, which varies from 2.3 to 7.3 nm across the investigated wavelength region, and (ii) the line width broadening induced by scattering due to surface roughness of the microspheres. Even minor surface imperfections (on the order of 2−8 nm) have been reported to significantly reduce WGM quality factors, typically by one to two orders of magnitude.[55] Such a reduction in Q broadens the line widths of individual resonances, causing neighboring WGM peaks to overlap and contributing to the convoluted experimental spectrum.

Across the 500−780 nm spectral window, experimentally measured quality factors (Q) ranged from 24 to 63, corresponding to FWHM values of 9−36 nm. For the simulations, the Q ranged from 364 to 1924, and the FWHM ranged from 0.3 to 2.1 nm. On average, the experimentally observed Q-factors were approximately 24 times lower than their simulated counterparts, an order-of-magnitude reduction consistent with the combined influence of finite laser bandwidth and surface-induced scattering losses in the physical system.[54,55]

To mimic the effects of laser spectral broadening and surface roughness in the simulations, we applied Lorentzian line shape broadening by convolving each WGM with a Lorentzian function centered at its resonance wavelength, using FWHM values extracted from the experimental spectrum. This procedure broadens the sharp resonances in the simulated spectrum (SI, Figure S7), yielding a broadened spectral profile that more closely resembles the experimental spectrum in Figure 2d; details are provided in section 4.4 of the SI.

Despite the differences in resonance sharpness, the simulated and experimental spectra exhibited excellent agreement in the resonant whispering-gallery mode wavelengths and the average mode spacing. The simulated mode spacing was 56 meV compared to 57 meV experimentally. The peak envelope, however, was centered at 561 nm in simulation and appeared red-shifted to 585 nm in experiment. This difference can be attributed to minor discrepancies in the assumed refractive indices of SiO_2, slight variations in the microsphere radius from nominal values, and differences in the excitation conditions, such as the exact beam focus position between the experimental and simulated configurations.

Having established the spectral characteristics and simulated mode profiles, we next examined how the coupled light propagates within the waveguide. Directionality was quantified as the fraction of in-coupled light guided forward, backward, or laterally, as schematically illustrated in Figure 4a. The wavelength dependence of these fractions is shown in SI, Figure S4c. At λ = 555 nm (Figure 4d), 46% of the incident light couples into the waveguide, of which 84% propagates forward, 13% laterally, and 3% backward. These fractions correspond to 39%, 6%, and 1% of the incident light in the respective channels (SI, Figure S4b). While the absolute coupling efficiency varied across WGMs, the forward channel consistently dominated, with an average of 88% of the coupled light traveling in the forward direction (Figure 4d). These results highlight the highly directional nature of the coupling, suggesting the potential of this platform for targeted light delivery to catalytic sites or optoelectronic devices at specific spatial locations.

https://doi.org/10.1021/acsphotonics.5c02800
ACS Photonics 2026, 13, 4966−4973

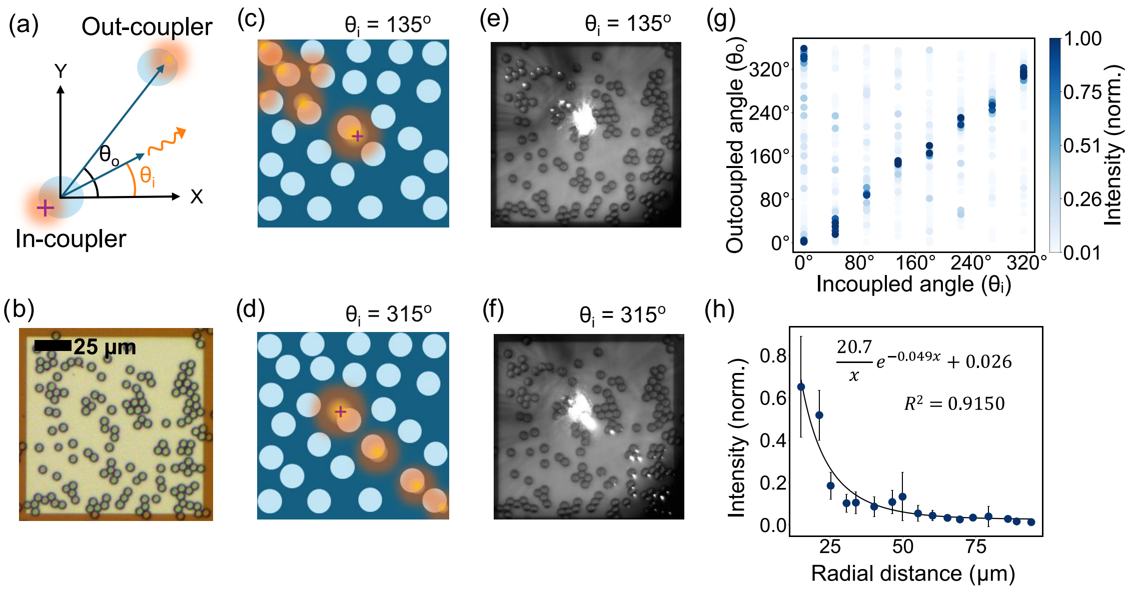

Figure 5. Directional out-coupled light from silica microspheres on the Si_3N_4 waveguide. (a) Schematic of laser positioning on the in-coupler microsphere, defining the in-plane launch angle θ_i and out-coupling angle θ_o. (b) Bright-field optical image of the waveguide with stamped SiO_2 microspheres. Schematics of light in-coupled at θ_i = 135° (c) and 315° (d), with corresponding experimental optical images (e, f) showing out-coupled light along the respective directions. (g) The intensity of light out-coupled from each microsphere on the waveguide, together with its corresponding out-coupling angle (θ_o), plotted as a function of in-coupling angle (θ_i). (h) Radial intensity of out-coupled light as a function of the distance from the in-coupling microsphere. Excitation angles θ_i are defined with an accuracy of ± 9° due to the finite beam radius ($\sigma \approx 0.38$ μm at λ = 550 nm) relative to the microsphere radius (2.5 μm).

Directional Out-Coupling

Numerical simulations of light in-coupling by a single SiO_2 microsphere revealed that light predominantly propagates in the forward direction. To investigate this behavior experimentally, multiple microspheres were deposited onto the waveguide (see section 1 of the SI for details), forming a uniform distribution. A single, isolated microsphere positioned near the center of the waveguide served as the in-coupler, while light out-coupled from neighboring microspheres was used to quantify the out-coupled intensity as a function of distance and angle from the in-coupler.

When the SiO_2 microsphere was excited with linearly polarized light at λ = 550 nm outside of the suspended membrane region of the substrate, no out-coupling was observed from neighboring microspheres, even from a microsphere only ~8.4 μm away from the illuminated sphere (SI, Figure S8a). This indicates that most of the light is absorbed by the underlying silicon before it can reach neighboring out-couplers. In contrast, when the microsphere was excited on the suspended Si_3N_4 membrane, strong out-coupling was observed from neighboring microspheres at distances up to ~50 μm, demonstrating efficient waveguiding via the low-loss suspended Si_3N_4 (SI, Figure S8b).

To achieve directional propagation, the laser is positioned at the edge of the in-coupler microsphere opposite to the intended direction of light travel. In Figure 5a, the purple crosshair marks the laser position on the rim of the in-coupler microsphere. The orange wavy arrow indicates the selected in-plane launch direction of light, θ_i, defined with respect to the in-coupler center. The out-coupling angle, θ_o, is defined from the same center as the in-plane azimuthal angle of the position vector connecting the in-coupler to each distal out-coupler. Owing to the uniform distribution of microspheres on the membrane (Figure 5b), the measured intensity and angular distribution of out-coupled light directly reflect the directionality of the guided light launched by the in-coupler.

Figure 5c,d schematically illustrate directional in-coupling achieved by edge-excitation, where downstream microspheres out-couple guided light. The corresponding optical images (Figure 5e,f), show light injected at θ_i = 135° and 315°, with out-coupling observed exclusively along the respective trajectories. In Figure 5g, the out-coupled light intensity and angle θ_o from various microspheres on the waveguide are plotted for different in-coupling angles θ_i (0°, 45°, 90°, 135°, 180°, 225°, 270°, 315°). A clear linear correlation is observed, indicating controlled directional propagation of waveguided light, in agreement with simulation results.

Additionally, the radial intensity of out-coupled light as a function of distance exhibits a decay profile characterized by both exponential attenuation, due to scattering by microspheres, and a $1/r$ dependence, consistent with 2D radial diffusion in slab waveguides.[56] This hybrid decay reflects the 2D nature of the guided mode, where light spreads laterally while being partially scattered at each microsphere, which acts as a localized out-coupling site (Figure 5h). From the fitted decay constant $L = 1/0.049 = 20.4$ μm (Figure 5h) and an average intersphere spacing $\Delta x = 10.3$ μm, the average out-coupling efficiency of the microspheres is estimated to be 40% at 550 nm (see Section 5.2 of the SI for details of calculation). This value closely matches the independently measured single-microsphere in-coupling efficiency of 42% at the same wavelength (SI, Figure S9), which is expected considering the reciprocity of light coupling and propagation within the system.[57]

As a proof of concept for reconfigurable photocatalysis, we tested whether guided light could excite localized surface plasmons in AuNCs deposited on the waveguide. A single microsphere in-coupler launched guided light toward the AuNCs, producing faint scattering spots that SEM confirmed to coincide with AuNC clusters (SI, Figure S11). These preliminary results demonstrate that the platform can deliver guided light to plasmonic nanoparticles, enabling on-chip plasmon-enhanced spectroscopy and photocatalysis.

■ CONCLUSION

We have introduced a lithography-free microsphere−waveguide coupling platform that efficiently transfers free-space light into suspended Si_3N_4 membranes. A single 5 μm SiO_2 microsphere achieves absolute in-coupling efficiencies up to 50%, with reproducible tuning of the dominant wavelength from 550−710 nm via axial beam translation. Directional out-coupling experiments further confirm that light can be steered along chosen trajectories, with the extracted out-coupling efficiency showing excellent agreement with the wavelength-matched in-coupling efficiency, consistent with reciprocity. Full-field simulations support the WGM-mediated coupling mechanism by reproducing the resonance spacing, modal field profiles, and directional launching of guided light.

By combining high efficiency, broadband operation, postfabrication tunability, and directional control, microsphere couplers offer a practical alternative to static lithographic devices. This platform provides a reconfigurable and straightforward route for visible light delivery in integrated photocatalysis, lab-on-chip spectroscopy, and other wavelength-selective nanophotonic applications.

■ ASSOCIATED CONTENT

Supporting Information

The Supporting Information is available free of charge at https://pubs.acs.org/doi/10.1021/acsphotonics.5c02800.

Experimental details, microsphere deposition, integrating-sphere microscopy setup, Lorentzian fitting procedures, FDTD simulation details, WGM mode assignments, simulated peak broadening, directional out-coupling analysis, repeatability measurement, and Au nanocube excitation experiment (PDF)

■ AUTHOR INFORMATION

Corresponding Author

Erik C. Garnett − *LMPV-Sustainable Energy Materials Department, AMOLF, Amsterdam 1098XG, The Netherlands; University of Amsterdam, Amsterdam 1098XH, The Netherlands;* orcid.org/0000-0002-9158-8326; Email: e.garnett@amolf.nl

Authors

Rohit B. Raj − *LMPV-Sustainable Energy Materials Department, AMOLF, Amsterdam 1098XG, The Netherlands*

Jaime Rivera − *LMPV-Sustainable Energy Materials Department, AMOLF, Amsterdam 1098XG, The Netherlands*

Esther Alarcón-Lladó − *LMPV-Sustainable Energy Materials Department, AMOLF, Amsterdam 1098XG, The Netherlands; University of Amsterdam, Amsterdam 1098XH, The Netherlands;* orcid.org/0000-0001-7317-9863

Sachin Kinge − *Materials Research and Development, Toyota Motor Europe, B1930 Zaventem, Belgium;* orcid.org/0000-0002-9149-7440

Complete contact information is available at: https://pubs.acs.org/10.1021/acsphotonics.5c02800

Funding

This work is part of the Advanced Research Center for Chemical Building Blocks, ARC CBBC, which is co-founded and co-financed by the Dutch Research Council (NWO) and the Netherlands Ministry of Economic Affairs and Climate Policy.

Notes

The authors declare no competing financial interest.

■ REFERENCES

(1) Butt, M. A.; Mateos, X. Strategic insights into integrated photonics: Core concepts, practical deployments, and future outlook. *Appl. Sci.* **2024**, *14* (14), No. 6365.

(2) Zhang, Z.; Zhang, S.; Liu, X.; Wei, Z.; Sharma, T.; Murugan, G. S.; Tsang, H. K.; Liu, T.; Cheng, Z. Integrated optical spectrometers on silicon photonics platforms. *Laser Photonics Rev.* **2025**, *19* (7), No. 2400155.

(3) Shekhar, S.; Bogaerts, W.; Chrostowski, L.; Bowers, J. E.; Hochberg, M.; Soref, R.; Shastri, B. J. Roadmapping the next generation of silicon photonics. *Nat. Commun.* **2024**, *15* (1), No. 751.

(4) Sun, P.; Reano, R. M. Cantilever couplers for intra-chip coupling to silicon photonic integrated circuits. *Opt. Express* **2009**, *17* (6), 4565−4574.

(5) Kopp, C.; Chelnokov, A. Fiber grating couplers for silicon nanophotonic circuits: Design modeling methodology and fabrication tolerances. *Opt. Commun.* **2009**, *282* (21), 4242−4248.

(6) Huang, M.; Ballato, J.; Peacock, A. C. Semiconductor core fibres: A scalable platform for nonlinear photonics. *npj Nanophotonics* **2024**, *1* (1), No. 21.

(7) Galán, J. V.; Sanchis, P.; Sánchez, G.; Martí, J. Polarization insensitive low-loss coupling technique between SOI waveguides and high mode field diameter single-mode fibers. *Opt. Express* **2007**, *15* (11), 7058−7065.

(8) Bhandari, B.; Im, C.-S.; Lee, K.-P.; Kim, S.-M.; Oh, M.-C.; Lee, S.-S. Compact and broadband edge coupler based on multi-stage silicon nitride tapers. *IEEE Photonics J.* **2020**, *12* (6), 1−11.

(9) Ai, X.; Xuan, M. W.; Zhang, Y.; Hsu, W.-L.; Veilleux, S.; Dagenais, M. Broadband high coupling efficiency edge coupler with low polarization-dependence on the silicon nitride platform. *Opt. Express* **2025**, *33* (7), 16253−16262.

(10) Cheng, L.; Mao, S.; Li, Z.; Han, Y.; Fu, H. Y. Grating couplers on silicon photonics: Design principles, emerging trends and practical issues. *Micromachines* **2020**, *11* (7), No. 666.

(11) Mu, X.; Wu, S.; Cheng, L.; Fu, H. Y. Edge couplers in silicon photonic integrated circuits: A review. *Appl. Sci.* **2020**, *10* (4), No. 1538.

(12) Wang, L.; Huang, Z.; Yang, X.; Rogée, L.; Huang, X.; Zhang, X.; Lau, S. P. Review on optofluidic microreactors for photocatalysis. *Rev. Chem. Eng.* **2023**, *39* (5), 765−782.

(13) Wang, N.; Zhang, X.; Wang, Y.; Yu, W.; Chan, H. L. W. Microfluidic reactors for photocatalytic water purification. *Lab Chip* **2014**, *14* (6), 1074−1082.

(14) Elmas, S.; Ambroz, F.; Chugh, D.; Nann, T. Microfluidic chip for the photocatalytic production of active chlorine. *Langmuir* **2016**, *32* (19), 4952−4958.

(15) Mayer, K. M.; Hafner, J. H. Localized surface plasmon resonance sensors. *Chem. Rev.* **2011**, *111* (6), 3828−3857.

(16) Mcoyi, M. P.; Mpofu, K. T.; Sekhwama, M.; Mthunzi-Kufa, P. Developments in localized surface plasmon resonance. *Plasmonics* **2025**, *20* (7), 5481−5520.

(17) Schneider, J.; Matsuoka, M.; Takeuchi, M.; Zhang, J.; Horiuchi, Y.; Anpo, M.; Bahnemann, D. W. Understanding TiO_2 photocatalysis: Mechanisms and materials. *Chem. Rev.* **2014**, *114* (19), 9919−9986.

(18) Chen, J.; Li, T.; An, X.; Fu, D. Photocatalytic reduction of CO_2 by TiO_2 modified materials: Recent advances and outlook. *Energy Fuels* **2024**, *38* (9), 7614−7636.
(19) Zhang, H.; Wang, J. J.; Fan, J.; Fang, Q. Microfluidic chip-based analytical system for rapid screening of photocatalysts. *Talanta* **2013**, *116*, 946−950.
(20) Meng, Y.; Chen, F.; Wu, C.; Krause, S.; Wang, J.; Zhang, D.-W. Light-addressable electrochemical sensors toward spatially resolved biosensing and imaging applications. *ACS Sens.* **2022**, *7* (7), 1791−1807.
(21) Chaudhary, G.; Dhwaj, A.; Verma, A.; Kumari, P.; Lal, K.; Verma, D.; Prabhakar, A. Sustainable and advanced LED-implanted microfluidic photoreactor with coupled optical fiber enabling efficient photocatalytic synthesis beside online reaction progress monitoring. *ACS Omega* **2024**, *9* (41), 42267−42277.
(22) Tao, P.; Ge, K.; Dai, X.; Xue, D.; Luo, Y.; Dai, S.; Xu, T.; Jiang, T.; Zhang, P. Fiber optic SERS sensor with silver nanocubes attached based on evanescent wave for detecting pesticide residues. *ACS Appl. Mater. Interfaces* **2023**, *15* (25), 30998−31008.
(23) Kong, L.; Lee, C.; Earhart, C. M.; Cordovez, B.; Chan, J. W. A nanotweezer system for evanescent wave excited surface enhanced Raman spectroscopy of single nanoparticles. *Opt. Express* **2015**, *23* (5), 6793−6802.
(24) Li, Y.; Lin, B.; Ge, L.; Guo, H.; Chen, X.; Lu, M. Real-time spectroscopic monitoring of photocatalytic activity promoted by graphene in a microfluidic reactor. *Sci. Rep.* **2016**, *6*, No. 28803.
(25) Gu, Y.; Xu, S.; Li, H.; Wang, S.; Cong, M.; Lombardi, J. R.; Xu, W. Waveguide-enhanced surface plasmons for ultrasensitive SERS detection. *J. Phys. Chem. Lett.* **2013**, *4* (18), 3153−3157.
(26) Braginsky, V. B.; Gorodetsky, M. L.; Ilchenko, V. S. Quality-factor and nonlinear properties of optical whispering-gallery modes. *Phys. Lett. A* **1989**, *137* (7−8), 393−397.
(27) Cai, M.; Painter, O.; Vahala, K. J. Observation of critical coupling in a fiber taper to a silica-microsphere whispering-gallery mode system. *Phys. Rev. Lett.* **2000**, *85* (1), 74−77.
(28) Shu, F.; Jiang, X.; Zhao, G.; Yang, L. A scatterer-assisted whispering-gallery-mode microprobe. *Nanophotonics* **2018**, *7* (8), 1455−1460.
(29) Tsintzos, S. I.; Tsimvrakidis, K.; Gates, J. C.; Elshaari, A. W.; Smith, P. G. R.; Zwiller, V.; Riziotis, C. Coupling nanowire quantum dots to optical waveguides by microsphere-induced photonic nanojet. *Photonics* **2024**, *11* (4), No. 343.
(30) Kushwaha, P. K.; Singh, K. Y.; Mahor, H. S.; Singh, P. K. Light coupling to waveguides via angularly tuned photonic nanojet. *Opt. Commun.* **2025**, *587*, No. 131938.
(31) Ogura, T. Surface light propagating in a dielectric thin film generated via micro-spheres. *Opt. Express* **2023**, *31* (14), 23198−23211.
(32) Romero-García, S.; Merget, F.; Zhong, F.; Finkelstein, H.; Witzens, J. Visible wavelength silicon nitride focusing grating coupler with AlCu/TiN reflector. *Opt. Lett.* **2013**, *38* (14), 2521−2523.
(33) Liu, J.; Huang, G.; Wang, R. N.; He, J.; Raja, A. S.; Liu, T.; Engelsen, N. J.; Kippenberg, T. J. High-yield, wafer-scale fabrication of ultralow-loss dispersion-engineered silicon nitride photonic circuits. *Nat. Commun.* **2021**, *12* (1), No. 2236.
(34) Ji, X.; Okawachi, Y.; Gil-Molina, A.; Corato-Zanarella, M.; Roberts, S.; Gaeta, A. L.; Lipson, M. Ultra-low-loss silicon nitride photonics based on deposited films compatible with foundries. *Laser Photonics Rev.* **2023**, *17* (3), No. 2200544.
(35) Vogt, D. W.; Jones, A. H.; Leonhardt, R. Free-space coupling to symmetric high-Q terahertz whispering-gallery mode resonators. *Opt. Lett.* **2019**, *44* (9), 2220−2223.
(36) Zambrana-Puyalto, X.; D'Ambrosio, D.; Gagliardi, G. Excitation mechanisms of whispering gallery modes with direct light scattering. *Laser Photonics Rev.* **2021**, *15* (5), No. 2000528.
(37) Gaber, N.; Malak, M.; Yuan, X.; Nguyen, K. N.; Basset, P.; Richalot, E.; Angelescu, D.; Bourouina, T. On the free-space Gaussian beam coupling to droplet optical resonators. *Lab Chip* **2013**, *13* (5), 826−833.
(38) Schinke, C.; Peest, P. C.; Schmidt, J.; Brendel, R.; Bothe, K.; Vogt, M. R.; Kröger, I.; Winter, S.; Schirmacher, A.; Lim, S.; Nguyen, H. T.; MacDonald, D. Uncertainty analysis for the coefficient of band-to-band absorption of crystalline silicon. *AIP Adv.* **2015**, *5* (6), No. 067168.
(39) Yang, S.; Wang, Y.; Sun, H. D. Advances and prospects for whispering gallery mode microcavities. *Adv. Opt. Mater.* **2015**, *3* (9), 1136−1162.
(40) Bohren, C. F.; Huffman, D. R. *Absorption and Scattering of Light by Small Particles*; Wiley: New York, 1998.
(41) Eremenko, Z. E.; Filipov, Y. F.; Kharkovsky, S. N.; Kutuzov, V. V.; Kogut, A. E. Whispering-gallery modes in shielded hemispherical dielectric resonators. *IEEE Trans. Microwave Theory Tech.* **2002**, *50* (11), 2647−2649.
(42) Himmelhaus, M.; Krishnamoorthy, S.; Francois, A. Optical sensors based on whispering gallery modes in fluorescent microbeads: Response to specific interactions. *Sensors* **2010**, *10* (6), 6257−6274.
(43) Kang, T. Y.; Lee, W.; Ahn, H.; Shin, D.-M.; Kim, C.-S.; Oh, J.-W.; Kim, D.; Kim, K. Plasmon-coupled whispering gallery modes on nanodisk arrays for signal enhancements. *Sci. Rep.* **2017**, *7*, No. 11737.
(44) Loyez, M.; Adolphson, M.; Liao, J.; Yang, L. From whispering gallery mode resonators to biochemical sensors. *ACS Sens.* **2023**, *8* (7), 2440−2470.
(45) Gorodetsky, M. L.; Ilchenko, V. S. Optical microsphere resonators: Optimal coupling to high-Q whispering-gallery modes. *J. Opt. Soc. Am. B* **1999**, *16* (1), 147−154.
(46) Cai, L.; Pan, J.; Hu, S. Overview of the coupling methods used in whispering gallery mode resonator systems for sensing. *Opt. Lasers Eng.* **2020**, *127*, No. 105968.
(47) Panitchob, Y.; Murugan, G. S.; Zervas, M. N.; Horak, P.; Berneschi, S.; Pelli, S.; Conti, G. N.; Wilkinson, J. S. Whispering gallery mode spectra of channel waveguide coupled microspheres. *Opt. Express* **2008**, *16* (15), 11066−11076.
(48) Boudoukha, R.; Perrin, S.; Demagh, A.; Montgomery, P.; Demagh, N.-E.; Lecler, S. Near- to far-field coupling of evanescent waves by glass microspheres. *Photonics* **2021**, *8* (3), No. 73.
(49) Murugan, G. S.; Panitchob, Y.; Tull, E. J.; Bartlett, P. N.; Hewak, D. W.; Zervas, M. N.; Wilkinson, J. S. Position-dependent coupling between a channel waveguide and a distorted microsphere resonator. *J. Appl. Phys.* **2010**, *107* (5), No. 053105.
(50) Cao, H.; Wiersig, J. Dielectric microcavities: Model systems for wave chaos and non-Hermitian physics. *Rev. Mod. Phys.* **2015**, *87* (1), 61−111.
(51) D'Ambrosio, D.; Zambrana-Puyalto, X.; Capezzuto, M.; Giorgini, A.; Malara, P.; Avino, S.; Gagliardi, G. Angular-momentum coupling of optical whispering-gallery modes to liquid droplet microresonators. *Phys. Rev. A* **2021**, *104* (4), No. 043504.
(52) Suebka, S.; McLeod, E.; Su, J. Ultra-high-Q free-space coupling to microtoroid resonators. *Light Sci. Appl.* **2024**, *13* (1), No. 75.
(53) Kavungal, V.; Farrell, G.; Wu, Q.; Mallik, A. K.; Semenova, Y. A comprehensive experimental study of whispering gallery modes in a cylindrical microresonator excited by a tilted fiber taper. *Microwave Opt. Technol. Lett.* **2018**, *60* (6), 1495−1504.
(54) Vasista, A. B.; Dias, E. J. C.; de Abajo, F. J. G.; Barnes, W. L. Role of symmetry breaking in observing strong molecule−cavity coupling using dielectric microspheres. *Nano Lett.* **2022**, *22* (16), 6737−6743.
(55) Lin, G.; Henriet, R.; Coillet, A.; Jacquot, M.; Furfaro, L.; Cibiel, G.; Larger, L.; Chembo, Y. K. Dependence of quality factor on surface roughness in crystalline whispering-gallery mode resonators. *Opt. Lett.* **2018**, *43* (3), 495−498.
(56) Hu, J.; Menyuk, C. R. Understanding leaky modes: Slab waveguide revisited. *Adv. Opt. Photonics* **2009**, *1* (1), 58−106.
(57) Potton, R. J. Reciprocity in optics. *Rep. Prog. Phys.* **2004**, *67* (5), 717−754.